Supplementary Information (SI) for ChemComm.
This journal is © The Royal Society of Chemistry 2026

Lattice Perturbation by Optically Inert Sc^{3+} Grants $NaGdF_4$ Upconversion Nanocrystals Giant Emission and Excitation-Gated Thermal Response

Guiping Ren[a,b], Zhijing Zhu[a], Yuenan Zhang[a], Jie Xing[a], Hao peng[a] ∗, Fang Yang[a] ∗, Aiguo Wu[a] ∗

[a] *Ningbo Key Laboratory of Biomedical Imaging Probe Materials and Technology, Laboratory of Advanced Theranostic Materials and Technology, Chinese Academy of Sciences (CAS) Key Laboratory of Magnetic Materials and Devices, Ningbo; Institute of Materials Technology and Engineering, Chinese Academy of Sciences, Ningbo 315201, China*
Zhejiang International Cooperation Base of Biomedical Materials Technology and Application, Zhejiang Engineering Research Center for Biomedical Materials, Ningbo Cixi Institute of Biomedical Engineering, Cixi 315300, China
[b] *University of Chinese Academy of Sciences, Beijing 100049, China*

∗ Corresponding author.
E-mail address: penghao@nimte.ac.cn; yangf@nimte.ac.cn; aiguo@nimte.ac.cn

Support Information

Experimental section

Materials

Gadolinium (III) chloride ($GdCl_3$, 99.9%), ytterbium (III) chloride hexahydrate ($YbCl_3 \cdot 6H_2O$, 99.9%), thulium (III) chloride hexahydrate ($TmCl_3 \cdot 6H_2O$, 99.9%), and holmium (III) chloride hexahydrate ($HoCl_3 \cdot 6H_2O$, 99.9%) were purchased from Macklin. Erbium (III) chloride hexahydrate ($ErCl_3 \cdot 6H_2O$, 99.9%), scandium (III) chloride (ScCl3, 99.9%), sodium hydroxide (NaOH, 98%), ammonium fluoride (NH_4F, 98%), and cyclohexane (AR, 99.5%) were sourced from Sigma-Aldrich. Oleic acid (90%) and 1-octadecene (90%) were acquired from Thermo Fisher, unless otherwise stated. All chemicals were used as received without further purification.

Synthesis procedure

Sc^{3+} and lanthanide ion (Er^{3+}, Yb^{3+}/Er^{3+}, Yb^{3+}/Tm^{3+}, or Yb^{3+}/Ho^{3+}) co-doped β-$NaGdF_4$ nanocrystals were prepared via a modified thermal decomposition route. In a typical procedure, 1 mmol of $LnCl_3 \cdot 6H_2O$ (Ln = Gd, Sc, and dopants), 6 mL oleic acid, and 15 mL 1-octadecene were combined in a three-neck flask. The mixture was heated to 150 °C under argon for 40 min to yield a clear solution. After cooling, 10 mL of methanol containing 4 mmol NH_4F and 2.5 mmol NaOH was added and stirred vigorously for 40 min. The slurry was then heated to 120 °C under vacuum for 30 min to remove solvents. Under nitrogen, the temperature was rapidly raised to 300 °C and held for 1 h. The resulting nanocrystals were precipitated with ethanol, collected by centrifugation (6,000 rpm), and finally redispersed in cyclohexane or dried at 60 °C for storage.

HRTEM

TEM samples were prepared by repeated centrifugation and washing (at least 3 times) with an ethanol/cyclohexane mixture. The samples were then ultrasonically dispersed in cyclohexane and drop-cast onto holey copper or molybdenum grids supported by an ultra-thin carbon film, followed by overnight drying. Nano-morphological were carried out using a Talos F200X transmission electron microscope (TEM) equipped with energy-dispersive spectroscopy (EDS), operating at 300 kV.

X-ray characterisation

X-ray diffraction (XRD) was performed for phase analysis of the nanoparticles using a Bruker D8 Advance diffractometer with Cu Kα radiation (λ = 1.5406 Å). Measurements covered a 2θ range of 10°–80° with a 0.02° step size and 7.27° min^{-1} scan rate. Dried nanoparticles were ground into a fine powder, pressed into a flat sample holder to ensure uniform X-ray penetration. Diffraction patterns were analyzed via MDI Jade 6.5 software: phase identification was confirmed against JCPDS reference patterns, and corresponding unit cell parameters were calculated.

Optical characterization

The upconversion luminescence (UCL) properties were characterized by steady-state, temperature-dependent, and time-resolved spectroscopy. Steady-state emission spectra were collected using a Horiba FL3-111 fluorescence spectrometer under continuous-wave diode laser excitation at 980 nm (0.296 W) or 1550 nm (0.052 W) with a ≈2 mm spot at a 45° incidence angle. Emission was detected perpendicularly with a PMT (1 nm resolution) from 400 to 850 nm. Temperature-dependent measurements were performed using a precision temperature-controlled stage (RT–500 K, ±1 K). Time-resolved decays were recorded on a Horiba Fluorolog-QM system equipped with pulsed lasers (980/1550 nm, 22 ms pulse width) and a TCSPC module (minimum response time 2666 ns). Decay curves were collected until 10,000 photon counts were reached in the peak channel and were fitted multi-exponentially to extract lifetimes.

Supplementary figures:

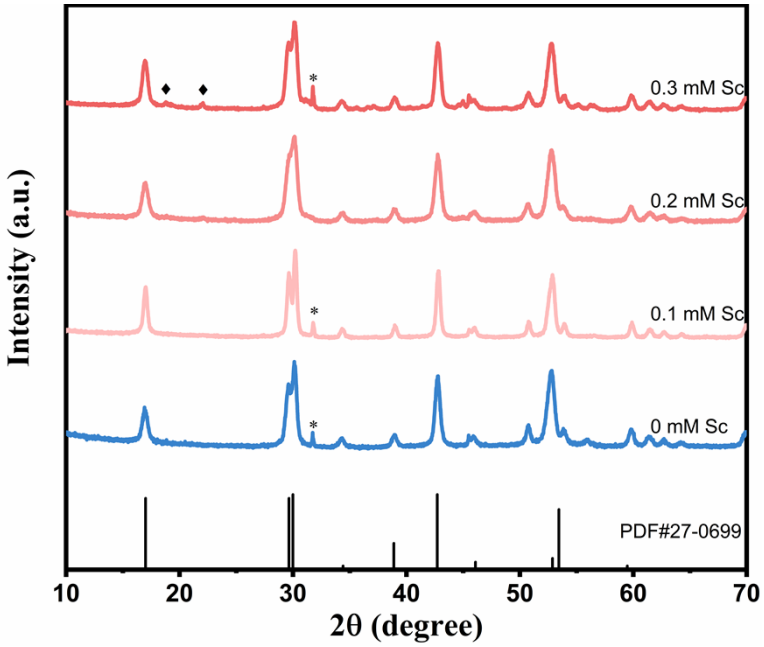

Figure.S1 Phase purity of $NaGdF_4$ nanocrystals with varying Sc^{3+} doping concentrations. XRD patterns show that the hexagonal $NaGdF_4$ phase (JCPDS No. 27-0699) is maintained up to 0.2 mM Sc^{3+}, above which (≥0.3 mM) characteristic peaks of a Na_3ScF_6 impurity phase (◆) emerge, defining the doping threshold for host lattice integrity. Peaks marked with * correspond to residual NaCl (JCPDS No. 05-0628) from synthesis precursors.

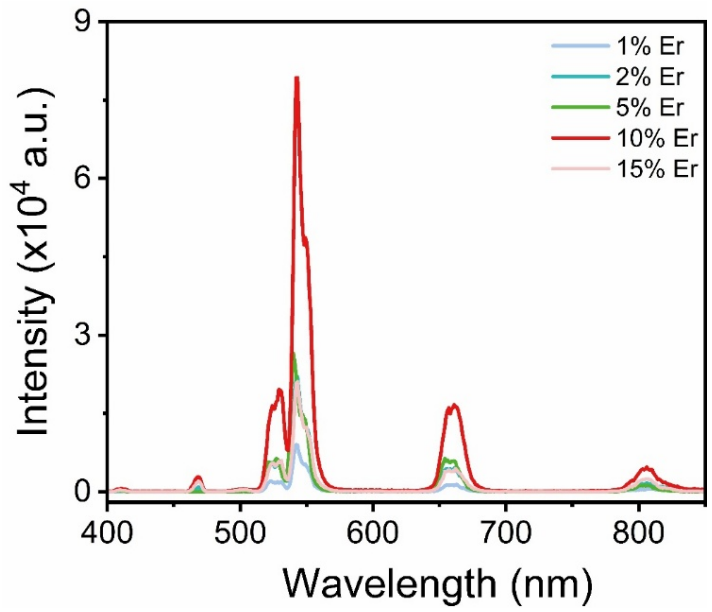

Figure S2. Concentration-dependent upconversion luminescence. Emission spectra of $NaGdF_4$:20%Sc/x%Er nanocrystals (x = 1,2, 5, 10, 15%) under 980 nm excitation. The luminescence intensity is enhanced with increasing Er^{3+} content up to 10%, but is quenched at 15%, establishing 10% as the optimum for achieving the brightest emission.

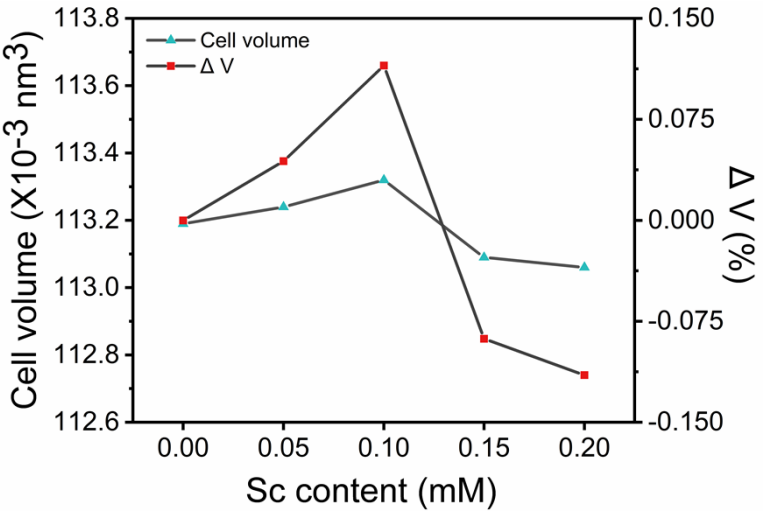

Figure S3. Lattice parameters of $NaGdF_4$:10%Er as a function of Sc^{3+} doping concentration. The unit cell volume exhibits a non-monotonic trend: it initially increases at low Sc^{3+} concentrations (<10 mol%) and then decreases at higher concentrations. This behavior supports the proposed dual-site incorporation

mechanism, where Sc^{3+} ions preferentially occupy interstitial sites at low concentrations (causing lattice expansion) and gradually switch to substitutional Gd^{3+} sites at higher concentrations (leading to lattice contraction).

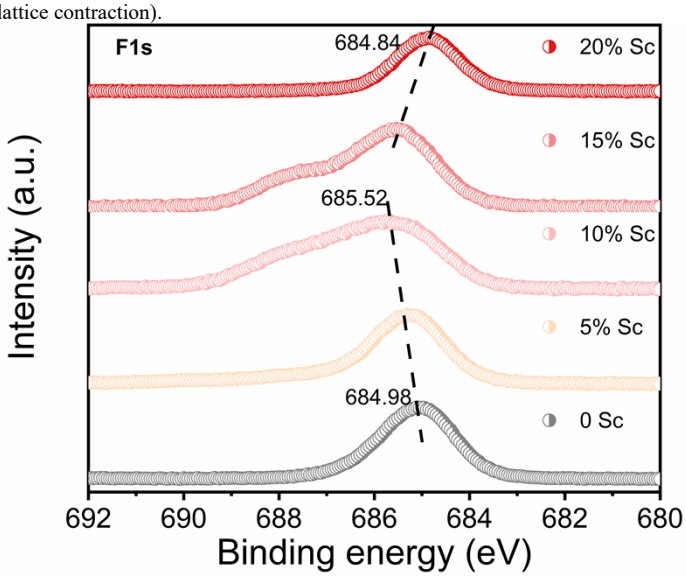

Figure S4. XPS F 1s spectra of $NaGdF_4$:10%Er nanocrystals as a function of Sc^{3+} doping concentration. The F 1s binding energy exhibits a non-monotonic shift with increasing Sc^{3+} content. The initial increase at low Sc^{3+} concentrations (<10 mol%) indicates that interstitial Sc^{3+} polarizes surrounding F^- ions, withdrawing electron density. The subsequent decrease at higher concentrations (>10 mol%) reflects relaxation of the local distortion as Sc^{3+} transitions to substitutional Gd^{3+} sites. This trend correlates with the lattice parameter evolution (Fig. S3) and provides direct chemical evidence for Sc^{3+}-induced modification of the local crystal field around Er^{3+} ions.

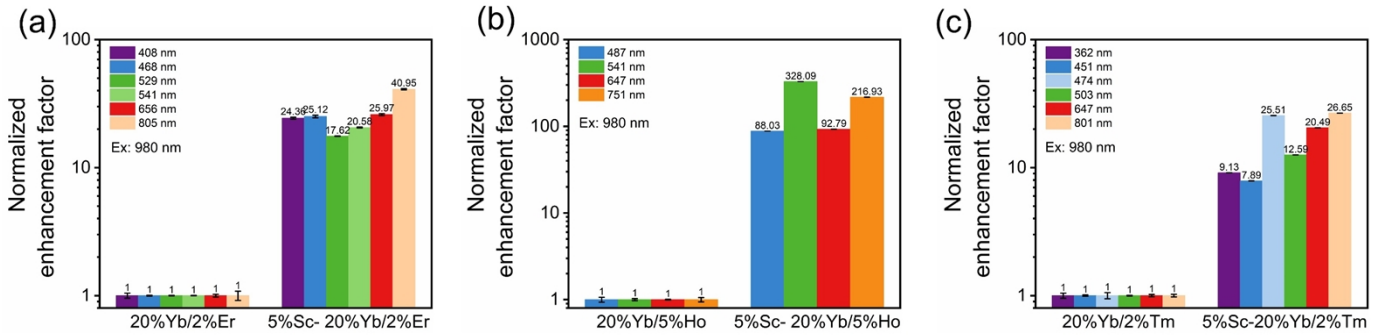

Figure S5. The enhanced upconversion emission of $NaGdF_4$:Yb/Er, Yb/Ho, and Yb/Tm systems with 5% Sc^{3+} doping under 980 nm excitation. Sc^{3+} incorporation significantly boosts the emission intensities of all three activator ions (17.62-40.95-fold for Er, 88.03-328.09-fold for Ho, and 7.89-26.65-fold for Tm), confirming that Sc^{3+}-induced crystal field modification is a versatile strategy for enhancing upconversion performance across different lanthanide-doped systems.

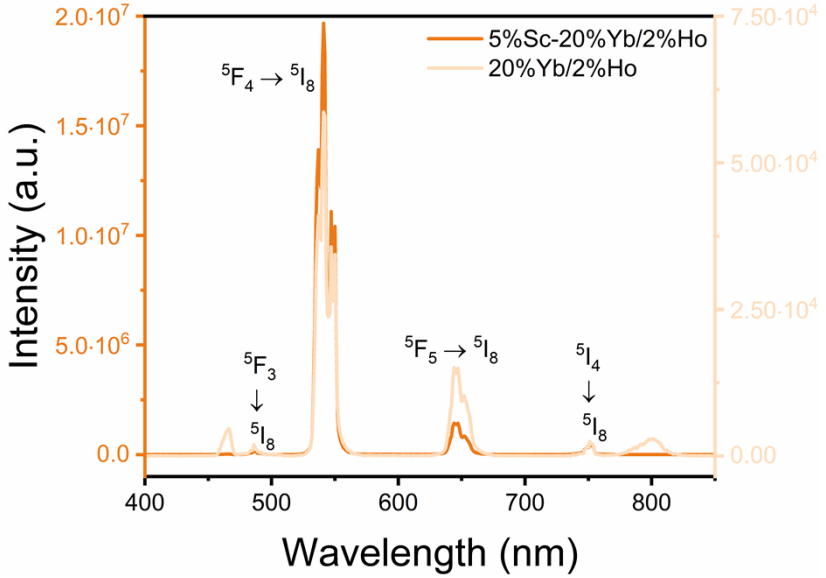

Figure.S6 The upconversion fluorescence emission spectrum of $NaGdF_4$:20%Yb/2%Ho and $NaGdF_4$:5%Sc/20%Yb/2%Ho excited at 980 nm were characterized. Experimental results demonstrate that the introduction of 5% Sc dopant can remarkably boost the intensity of upconversion emission peaks by 2-3 orders of magnitude. Specifically, the emission at 541 nm shows a prominent enhancement effect, while the intensities of other emission peaks are relatively weak, which endows the sample with distinct single-wavelength upconversion emission features.

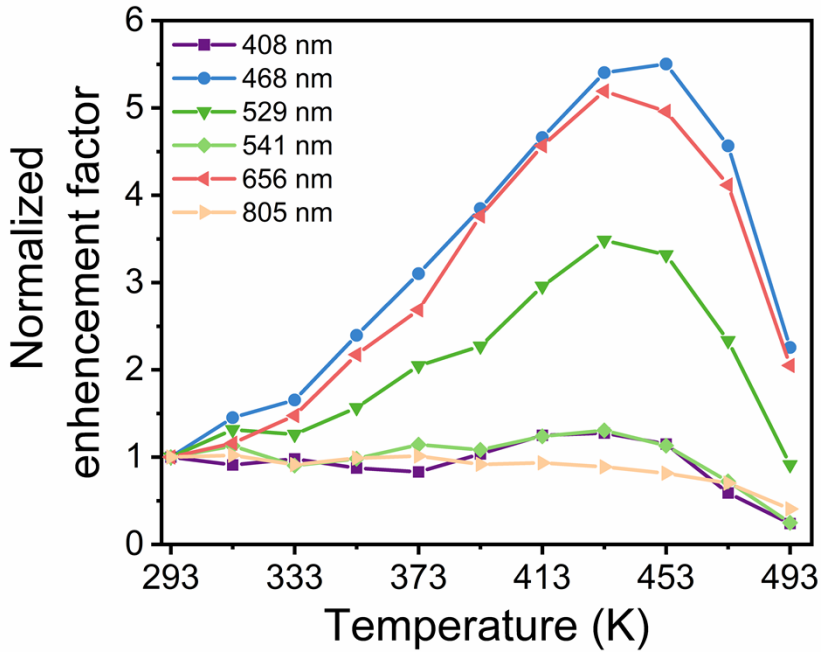

Figure S7. Temperature-dependent upconversion emission intensity of $NaGdF_4$:10%Er/5%Sc under 1550 nm excitation.

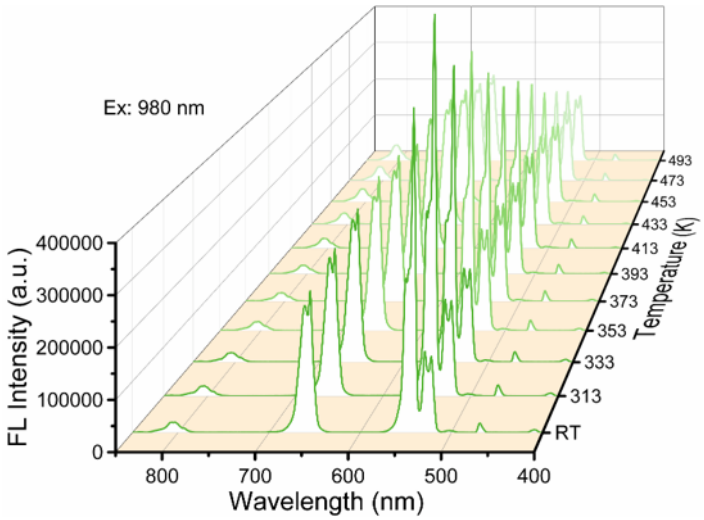

Figure S8. Temperature-dependent (RT-493K) upconversion emission spectra of $NaGdF_4$:10%Er/5%Sc nanocrystals under 980 nm excitation.

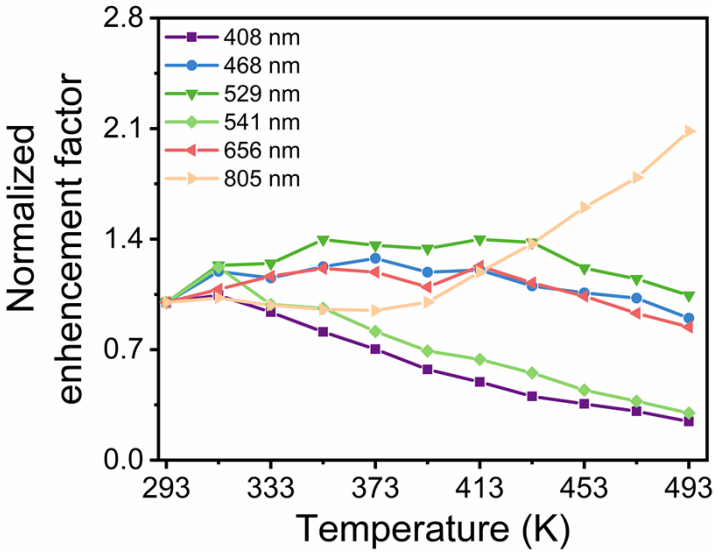

Figure S9. Temperature-dependent upconversion emission intensity of $NaGdF_4$:10%Er/5%Sc under 980 nm excitation.

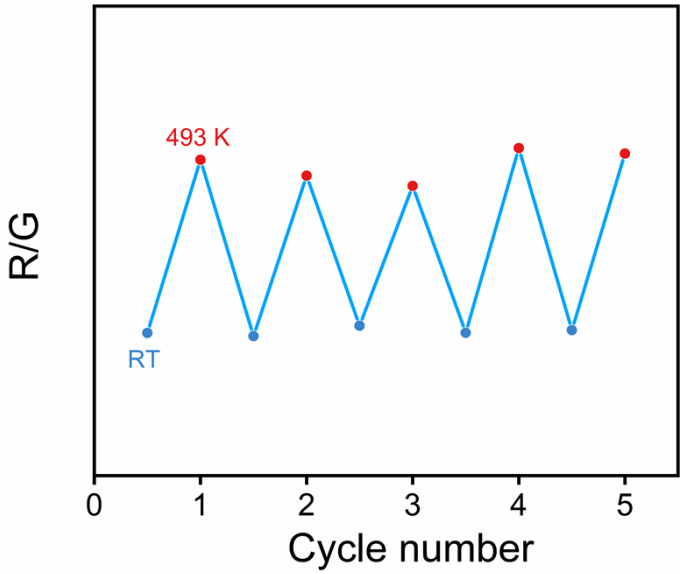

Figure S10. Stability assessment of the colorimetric response under 1550 nm excitation.

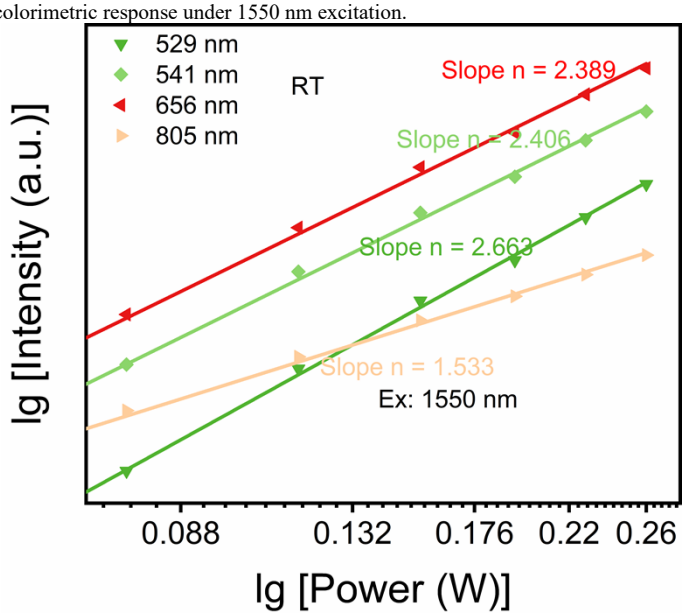

Figure S11. Double-logarithmic plots of upconversion intensity (I_{up}) versus laser power (P) under 1550 nm excitation at room temperature.

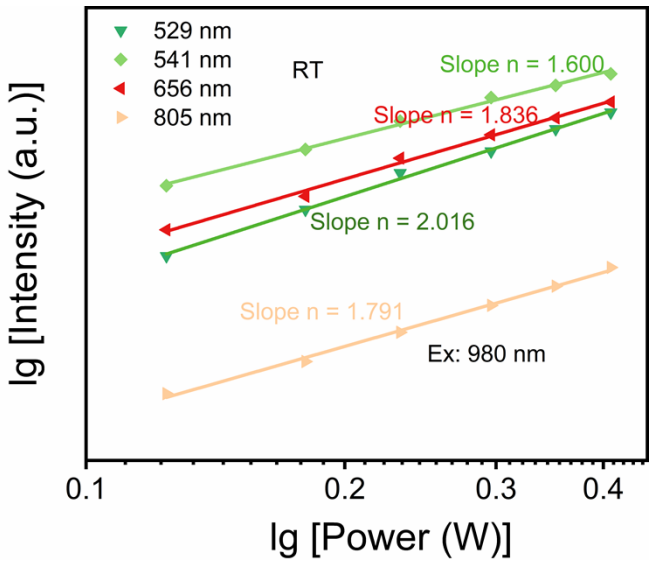

Figure S12. Double-logarithmic plots of upconversion intensity (Iup) versus laser power (P) under 980 nm excitation at room temperature.

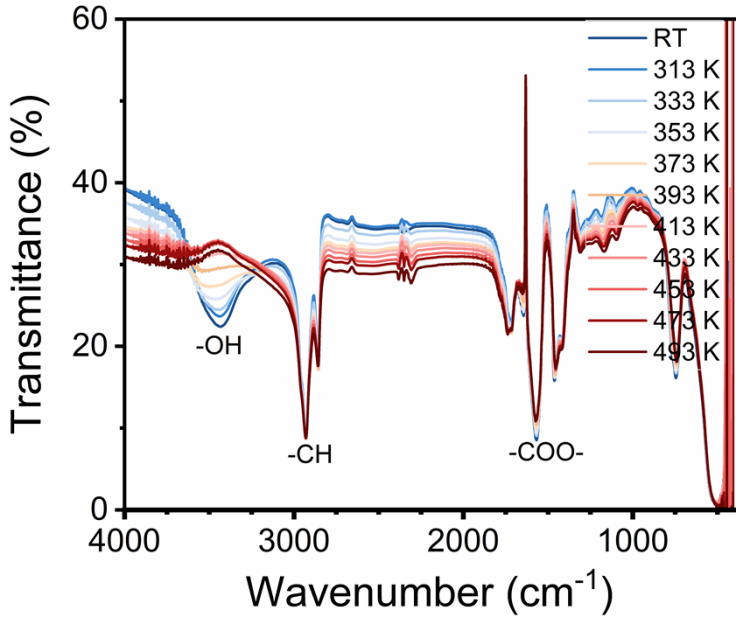

Figure S13. In situ Fourier transform infrared spectra of $NaGdF_4$:10% Er/5% Sc nanoparticles recorded at temperatures ranging from room temperature to 493 K.

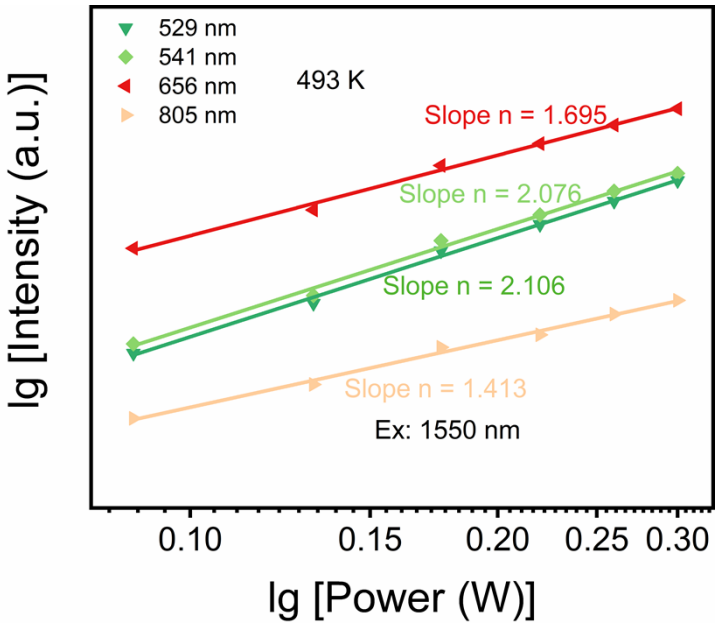

Figure S14. Double-logarithmic plots of I_{up} vs. P under 1550 nm excitation measured at 493 K.

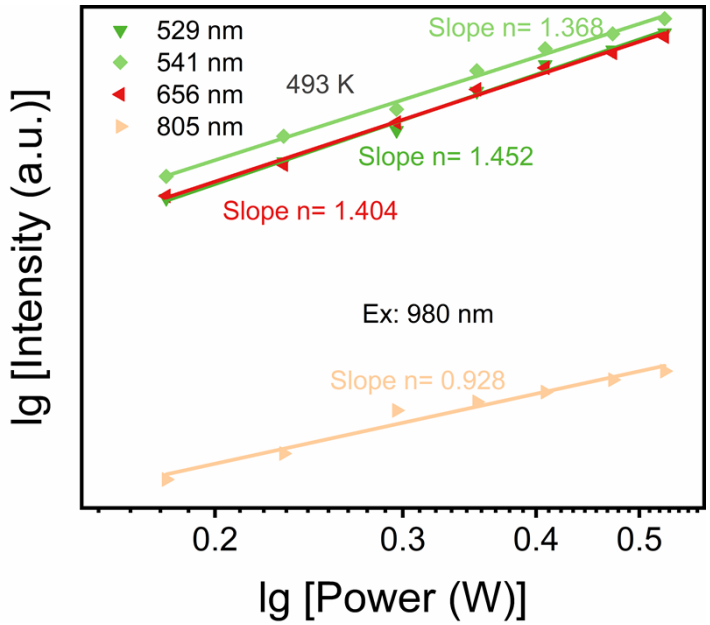

Figure S15. Double-logarithmic plots of I_{up} vs. P under 1550 nm excitation measured at 493 K.

Supplementary figures:

Table.S1 The chromaticity coordinates corresponding to the upconversion fluorescence emission of $NaGdF_4$:5%Sc/10%Er as a function of temperature were investigated under 980 nm and 1550 nm excitation, respectively. Results show that the sample exhibits a slight color variation under 980 nm excitation, while the upconversion emission color undergoes a remarkably large variation with temperature under 1550 nm excitation.

Temprature	CIE chromaticity coordinates (980 nm Ex)	CIE chromaticity coordinates (1550 nm Ex)
RT	(0.290, 0.677)	(0.304, 0.661)
313 K	(0.285, 0.682)	(0.301, 0.662)
333 K	(0.290, 0.674)	(0.320, 0.636)
353 K	(0.287, 0.675)	(0.337, 0.617)
373 K	(0.288, 0.672)	(0.336, 0.614)
393 K	(0.287, 0.669)	(0.360, 0.586)
413 K	(0.291, 0.664)	(0.360, 0.585)
433 K	(0.289, 0.665)	(0.360, 0.583)
453 K	(0.291, 0.569)	(0.363, 0.575)
473 K	(0.289, 0.658)	(0.380, 0.553)
493 K	(0.288, 0.657)	(0.406, 0.519)